Appendix A

Air Čerenkov Detection of EeV/ZeV cosmic rays with Solar Panels or PMTs

A.1 Introduction

The strongest signal generated by an Extensive Air Shower (EAS) in the atmosphere is the Čerenkov light emitted by charged particles. This signal is 3 to 7 orders of magnitude larger than the ground level particle flux or the nitrogen fluorescence signal. This extremely bright light has some unusual properties, especially for EeV/ZeV (1 ZeV = 10^{21} eV) energy cosmic rays.

One unusual property is the sheer magnitude of the Čerenkov light yield. A 100 EeV shower is brighter than fluctuations in the direct daytime sun over the Čerenkov light emission time scale, even when observed several kilometers from the shower axis. This extraordinary intensity allows one to optically observe 100 EeV cosmic rays during observation conditions with new moon, full moon, dusk, dawn, and possibly during the daytime. This capability overcomes the typical 10-15% duty cycle limitation of other optical (nitrogen fluorescence) detection techniques.

Another interesting consequence of the high Čerenkov photon flux is the ability to use low cost silicon detectors to observe the signal. A 10^{20} eV cosmic ray shower creates a Čerenkov signal strong enough to generate a milliamp current pulse in a large (1 m^2) solar panel, even when the solar panel is hundreds of meters away from the core of the EAS. Such large current pulses can be easily detected with existing low cost commercial electronics. Commercial PIN diodes (1 cm^2 area) can provide even stronger signals since their inherent electronic noise is substantially smaller than that of solar panels. Low gain photomultipler tubes, using only a few dynodes for photoelectron amplification, provide another method of detecting the bright Čerenkov light, and could extend the detection threshold to even lower cosmic ray energies.

The use of silicon detectors gives the detector the ability to detect Čerenkov light at long wavelengths (600-1000 nm), where Rayleigh scattering and atmospheric attenuation is small. This sensitivity allows detection of cosmic rays at substantially larger zenith angles than the particle array, possibly up to 80-85°. One may be able to use this steep angle detection capability to look for astrophysical sources of high energy neutrinos. This capability would not be achievable with a low gain PMT, since these devices are generally not sensitive to long wavelengths.

This capability complements the detection aperture of the nitrogen fluorescence detector, which also has the capability to detect air showers at steep zenith angles. An array of air Čerenkov detectors could provide additional information for hybrid reconstruction of these steep zenith angle events which would not trigger the particle detector array. The longer wavelength detection bandwidth also reduces sensitivity to atmospheric conditions for more normal, near vertical showers.

The narrow 'beamed' nature of the Čerenkov light provides a novel method for reconstruction of the direction of the original cosmic ray. Multiple flat light sensors are used at a single site to observe different hemispheres of the sky. The beamed light will illuminate the flat surfaces with different amounts of light, depending upon their orientation with respect to the incoming light beam. The sensor amplitudes can therefore be used to reconstruct the original Čerenkov light and cosmic ray direction with an accuracy of 0.5°- 2°, similar to or better than the surface particle detector array.

Perhaps the most important attribute of Čerenkov light is its usefulness in energy determination. Čerenkov light provides a direct calorimetric measurement of the total energy of the EAS. The expected energy resolution is expected to be 10-35%, depending upon the zenith angle of the primary. The Čerenkov light lateral distribution also possesses information about the depth of the shower maximum (X_{max}), and may allow determination of the cosmic ray primary composition.

A novel idea under consideration is the use of large solar panels for power generation during full daylight and for Čerenkov light detection at other times. This "dual-use" of the panels, combined with the elimination of the traditional high voltage supplies associated with PMTs, may allow the construction of an "add-on" solar panel Čerenkov array detector at a very low cost.

We describe here some of the capabilities of a "strawman" air Čerenkov detector design for the Auger project. The detector can easily be added to the water Čerenkov particle detector array as the mechanical and power requirements of the air Čerenkov detectors are minimal. From our Monte Carlo simulations of this strawman design, we demonstrate that a relatively simple air Čerenkov detector can work well as a stand-alone system, as well as an add-on detector to the Auger ground array system.

It is impossible to fully describe the Čerenkov array concept and design considerations in this paper due to page limitations. Instead, we will focus on the the most pertinent factors in the design of this detector. A full description of the concept of observation of 100 EeV energy cosmic rays with Čerenkov light and silicon detectors has been described elsewhere [154]. A full paper providing details of the geometric reconstruction technique for a standalone silicon sensor Čerenkov array has been published[155]. Additional considerations on the signal and noise considerations for silicon devices has also been published elsewhere[156].

A.2 Some Key Design Considerations

Signal and Noise levels The Signal-to-Noise (S/N) ratio is the key parameter for how well one will be able to determine cosmic ray direction, energy, and composition. Figure A.1 plots the S/N ratio of the Čerenkov signal as a function of zenith angle, energy, and various background sky light conditions. This plot assumes a proton primary, a 5 μ sec integration of an 0.8 m^2 area light sensitive silicon panel (CZ-Si solar panel), and a 1 km perpendicular distance from the shower axis at ground level. This figure uses the calculated Čerenkov light spectra, and the known solar and lunar light spectra (AM1.5) multiplied by the wavelength dependent quantum efficiency of the solar panel and integrated between 300 and 1200 nm. A realistic (wind-driven aerosol) atmospheric transmission model is used in the calculation of the Čerenkov light spectrum. The noise levels in this figure include only statistical fluctuations in the sky background. The effect of inherent electronic noise levels in the silicon will be discussed later.

For nearly vertical showers, S/N does not scale with energy. It rises more slowly than a linear increase with energy. At these energies , vertical EAS strike the ground level near their X_{max}, resulting in a loss of Čerenkov light from electrons which normally would radiate light at steeper zenith angles. Higher energy events have deeper X_{max}, and therefore as energy increases, a larger percentage of the shower energy is lost into the ground level, resulting in a suppression of the available Čerenkov light from a linear increase with energy.

In what follows, the above figure can be consulted to relate the S/N to the cosmic ray primary energy and sky conditions. In this curve, we have made an assumption about the area of the optical detector, it's quantum efficiency, internal gain, and optimal integration time. The values used in the calculation were appropriate for the solar panel light sensor, however these measurements might be made with a number of different optical sensors (to be described later in this section).

To use the above S/N curve with other types of optical sensors, one needs to scale the S/N ratio by a factor

$$K = \sqrt{(\frac{A}{0.8m^2})(\frac{5\mu sec}{\Delta t})(\frac{QE}{0.6})(\frac{G}{1})} \tag{A.1}$$

where A is the detector area in m^2, QE is the average quantum efficiency integrated over the Čerenkov /background light spectrum, G is the internal gain of the light sensor and Δt is the optimal integration time in μ sec. For a 1 cm^2 area PIN diode sensor, $K \approx 1/10$; for a 4 inch diameter PMT run with a gain of 100, $K \approx 1$.

Detector On-Time Using the known amounts of no-moon, full moon, twilight, and day-time sun conditions for a 45 degree latitude Northern hemisphere site, we can predict the percentage of time that a minimum S/N of 10 is possible. Figure A.2 illustrates the possible

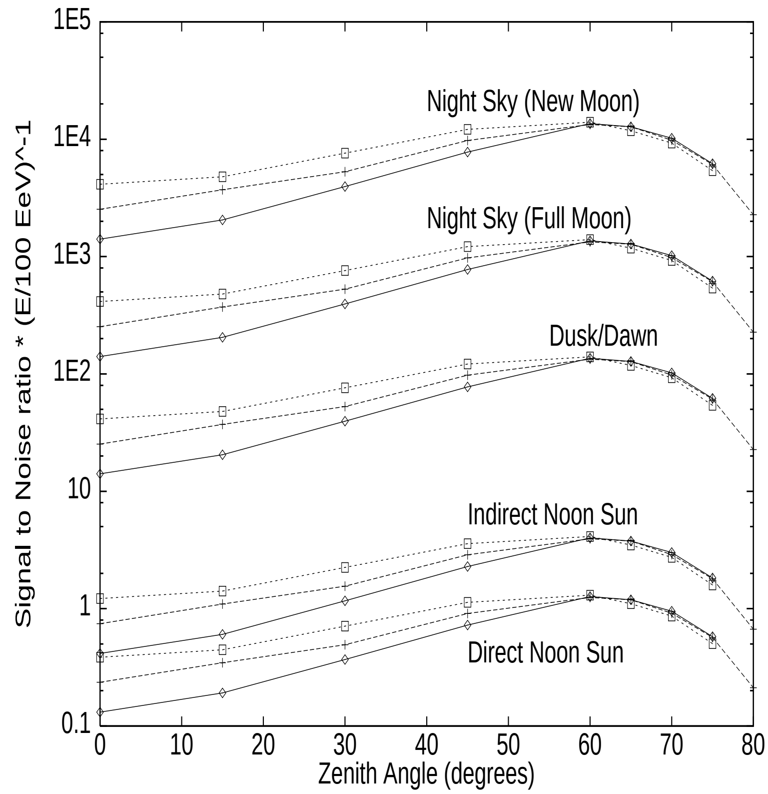

Figure A.1: Signal and Noise for Solar Panel detector at 1 km perpendicular distance from the shower axis as a function of zenith angle, primary energy, and various sky conditions. Primary Energies: Solid Lines with diamonds : 1000 EeV; Long Dash with Crosses: 100 EeV; Short Dashes with Boxes: 10 EeV. Horizontal Axis: Zenith angle (degrees); Vertical Axis: Energy scaled Signal-to-Noise ratio $S/N \times (\mathrm{E}/100\ \mathrm{EeV})^{-1}$.

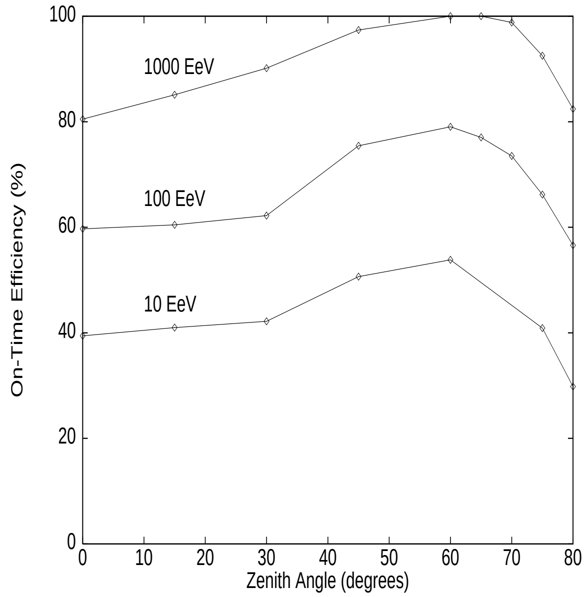

Figure A.2: On-Time efficiency for a 0.8 m^2 area solar panel detector located one km from the shower core as a function of primary energy and zenith angle. On-Time efficiency is defined as percentage time that the detector has a minimum S/N ratio of 10. Horizontal Axis: Zenith Angle (degrees) ; Vertical Axis: On-Time efficiency (%).
.

duty cycle as a function of primary energy and zenith angle for a 4 in diameter PMT (with extended IR response) or large solar panel detector which is 1 km from the core of the shower. The noise is due only to fluctuations in the sky background. One notes that for 10^{20} eV cosmic rays,a 60% duty cycle is easily achieved over almost all zenith angle trajectories. At 10^{21} eV, one approaches nearly 100% duty cycle for zenith angles between 40 to 70 degrees. The plot here assumes perfect weather, and should be compared to the canonical maximum 14% duty cycle typical of most air Čerenkov experiments.

For 1 cm^2 area PIN diodes (without Winston cones) , one must decrease the on time efficiency by about 20% for each curve to account for the reduced S/N for the devices (mainly due to their smaller area). We expect this type of sensor would provide a duty cycle of about 20-30% at 10 EeV, 40-50% at 100 EeV, and 60-70% at 1 ZeV. A PIN diode with a small Winston cone might increase the signal by a factor of 10, giving an increased duty cycle similar to the solar panel duty cycle. A PMT without red sensitivity would have a substantially reduced duty cycle above 65°due to the increased Rayleigh scattering of the short wavelengths to which the PMT is most sensitive. This would likely decrease the duty cycle by 20% at 60°zenith angle, and decrease it further by about 50-70% at 80°.

Choice of Optical Sensors and Inherent Noise Levels There are several choices for the optical detector for the air Čerenkov array: photomultiplier tubes (PMTS), solar cell panels, PIN diodes, and avalanche photodiodes (APD's). Since APD's are generally small area devices, and are quite expensive (Typically \$600-1000 each, about a factor of 10 more expensive for the same gain×area product as PIN diodes), we do not consider APD's to be a cost effective option.

PMTS can be used if the gain of the PMT is reduced to the order of 100 by disabling all but the first few dynodes. This has been successfully demonstrated[157]. PMTS generally do not have an extended wavelength sensitivity into the red. Large (0.8 m^2) panels of single crystal CZ-Si solar panels are another possibility for the optical detection element. Initial tests with large solar panels have indicated the capability to detect 800 nsec wide pulses of $< 10^8$ photons. The main limitation on these solar panels is the inherent electrical noise due to the poor quality of the silicon used in the device which leads to a large capacitance in the semiconductor p-n junction. This large capacitance makes it difficult to impedance match the detector to the preamplifier without introducing excessive noise. PIN diodes are made of substantially better quality silicon, have substantially lower capacitance per unit area than solar cells, and can be reverse biased to improve their linearity and decrease their capacitance. The choice between all of these different options depends upon the wavelength sensitivity , area cost, and relative noise level in the device.

In short, there are trade-offs between detector area, quantum efficiency, spectral sensitivity, internal signal gain, cost and inherent noise levels which makes different detectors advantageous in different situations.

Consider a generic light sensor with area A, wavelength dependent quantum efficiency $qe(\lambda)$ and internal gain G. If $\frac{dN_{ch}(\lambda)}{d\lambda}$ is the wavelength dependent Čerenkov photon flux, the photoelectron signal S generated by the sensor is

$$S = (A)(G) \int \frac{dN_{ch}(\lambda)}{d\lambda} qe(\lambda) d\lambda \tag{A.2}$$

The noise background is calculated from the combination of the statistical fluctuations in the sky background light level N_{sky} , the statistical fluctuation in the signal level N_{signal}, and the inherent (electronic) noise level in the sensor N_{inh}. The total noise level N is the quadrature sum of these three components,

$$N^2 = N_{sky}^2 + N_{signal}^2 + N_{inh}^2. \tag{A.3}$$

In making measurements of the Čerenkov light with strong background light (full moon, or even daylight), the signal S is on the order of 10^6 to 10^8 photoelectrons, whereas the the noise fluctuations in the sky background N_{sky} are typically 10^5 to 10^8 photoelectrons. Therefore the statistical fluctuation in the signal level $N_{signal} = \sqrt{S}$ is substantially less than N_{sky} and can be ignored.

The fluctuations in the sky background light level is given by

$$N_{sky} = \sqrt{(A)(G)(\Delta t) \int \frac{d^2 N_{sky}(\lambda)}{d\lambda dt} qe(\lambda) d\lambda} \tag{A.4}$$

where Δt is the optimal integration time for the Čerenkov photon pulse, and $\frac{d^2 N_{sky}(\lambda)}{d\lambda dt}$ is the wavelength dependent sky background photon flux per unit time.

The inherent (electronic) noise level in the sensor N_{inh} depends upon the type of sensor being used. For PMT measurements under intense light conditions, the usual sources electronic noise (spontaneous photoelectron emission, fluctuations in the gain at the first dynode) are dominated by the statistical fluctuations in the DC current through the tube ($= N_{sky}$) and therefore can be ignored.

For silicon detectors, the main source of noise is due to the large junction capacitance of the P-N junction of the sensor. The capacitance C_d of the sensor is related to the bulk resistivity ρ of the silicon used in the semiconductor device, and the sensor (junction) area A :

$$C_d = A\sqrt{\varepsilon/(2\mu_h\rho(V_0+V_b))} \tag{A.5}$$

where $\varepsilon = 1.054^{-10}$ is the permittivity of the silicon material, $\mu_h = 500cm^2V^{-1}sec^{-1}$ is the hole mobility in silicon, ρ is the bulk resistivity, $V_0 = 1V$ is the contact potential, and V_b is the externally applied junction (reverse) bias voltage. Inserting these factors gives

$$C_d = \frac{0.034A(cm^2)\mu F}{\sqrt{\rho(\Omega cm)(1+V_b(Volts))}}. \tag{A.6}$$

This capacitance will limit the amount of charge transferred from the optical sensor to the input of the preamplifier circuit. Transformers and high capacitance FET's are typically used to match impedances between a high capacitance sensor and the low capacitance preamplifier. The typical RMS equivalent noise N_{inh} for an optimally coupled detector with capacitance C_d, and assuming a signal resolving time on the order of 100 nsec [158], is

$$N_{inh} = 3\times10^5\sqrt{C_d(\mu F)}\ \text{RMS e}^- \tag{A.7}$$

Using the above numbers for the capacitance of the P-N junction gives an equivalent noise in the panel of approximately

$$N_{inh} = 3\times10^5\sqrt{A\sqrt{\varepsilon/(2\mu_h\rho(V_0+V_b))}} \tag{A.8}$$

$$= \frac{5.5\times10^4\sqrt{A(cm^2)}}{(\rho(\Omega cm)(1+V_b(Volts)))^{0.25}}\ \text{RMS e}^- \tag{A.9}$$

For a typical single crystal (CZ-Si) solar panel, $\rho = 1\Omega cm$, giving a capacitance per unit area of 0.034 $\mu F cm^{-2}$. This value has been experimentally measured at the University of Utah and has been found to be in good agreement with the above calculation. For a solar panel of $0.4m^2$ effective area, this gives an equivalent noise charge of about $N_{inh} = 3.5\times10^6e^-$. This noise level is similar to that induced in the panel by fluctuations in the DC photon level during twilight/sunrise sky conditions.

PIN diodes have substantially larger bulk resistivity ($\geq 10^3\Omega cm$) and therefore substantially lower capacitance per unit area. This results in the possibility of using reverse bias on the device to decrease the junction capacitance further, and improve device linearity at high illumination levels. The area of these devices, however, is substantially smaller than the solar panels, which will reduce the S/N for these devices.

We can examine the effect of the area vs. bulk resistivity trade-off in the S/N ratio quantitatively. The total S/N ratio for the sensor is derived by combining equations A.2, A.3, A.4 and A.8.

$$S/N = \frac{(A)(G)\int \frac{dN_{ch}(\lambda)}{d\lambda} qe(\lambda)d\lambda}{\sqrt{(A)(G)(\Delta t)\int \frac{d^2N_{sky}(\lambda)}{d\lambda dt} qe(\lambda)d\lambda + 9\times 10^{10} A\sqrt{\varepsilon/(2\mu_h \rho(V_0+V_b))}}} \tag{A.10}$$

We make the the approximations

$$N_{ch} < QE >_{ch} = \int \frac{dN_{ch}(\lambda)}{d\lambda} qe(\lambda)d\lambda \tag{A.11}$$

and

$$\frac{dN_{sky}}{dt} < QE >_{sky} = \int \frac{d^2N_{sky}(\lambda)}{d\lambda dt} qe(\lambda)d\lambda \tag{A.12}$$

where N_{ch} is the integrated number of Čerenkov photons over all wavelengths per unit area, $< QE >_{ch}$ is the average quantum efficiency of the sensor to the Čerenkov spectrum, dN_{sky}/dt is the background sky light level per unit time per unit area, integrated over all wavelengths, and $< QE >_{sky}$ is the average quantum efficiency of the sensor for viewing the sky spectrum.

Using these approximations, equation A.10 simplifies to

$$S/N = \frac{N_{ch} < QE >_{ch}}{\sqrt{\frac{dN_{sky}}{dt} < QE >_{sky} (\Delta t)}} \frac{\sqrt{(A)(G)}}{\sqrt{1 + \frac{9\times 10^{10}\sqrt{\varepsilon/(2\mu_h\rho(V_0+V_b))}}{(\Delta t)\frac{dN_{sky}}{dt} < QE >_{sky} (G)}}} \tag{A.13}$$

The factor on the right hand side of equation A.13 is

$$\frac{N_{ch} < QE >_{ch}}{\sqrt{\frac{dN_{sky}}{dt} < QE >_{sky} (\Delta t)}} \sqrt{(A)(G)} \tag{A.14}$$

This is essentially the the S/N ratio which depends only upon the energy of the cosmic ray, zenith angle of the cosmic ray, and sky background conditions. The variation of this S/N ratio as a function of these parameters has already been outlined in Figure A.1.

The remaining important factor in Equation A.13 is

$$\xi = \frac{9\times 10^{10}\sqrt{\varepsilon/(2\mu_h\rho(V_0+V_b))}}{(\Delta t)\frac{dN_{sky}}{dt} < QE >_{sky} (G)} \tag{A.15}$$

which determines the further degradation of the S/N ratio listed in Figure A.1 due to inherent electronic noise in the sensor. ξ is the ratio of the capacitance per unit area to the sky background fluctuations per unit area. If this ratio is very small , decreases in sky background fluctuations (going from daylight to dusk to moonless nights, etc) will result in real increases in S/N (the S/N is dominated by sky background). If ξ is large, then S/N does not improve as sky background fluctuations decrease (S/N is dominated by electronic noise).

We can calculate ξ for the CZ-Si, PIN diode , and PMT detectors using the known detector properties and parameters. If we examine the *ratio* of ξ for two different detectors, we will have a quantitative comparison of the difference in achievable S/N for different detectors. Using measured parameters and operating conditions for 0.4 m^2 effective area CZ-SI solar panel, a Hammamatsu S3590 (1 cm^2 area) PIN diode, and a 4 inch diameter, gain 100 bialkali PMT, we derive

$$\xi_{CZ-SI}/\xi_{PIN} = 270$$

and

$$\xi_{CZ-SI}/\xi_{PMT} = 2 \times 10^4.$$

These ratios demonstrate the relative amounts of noise in each sensor without regard to the actual detection area, gain, or quantum efficiency.

Accounting for the differences in area, gain , quantum efficiency and sensitivity between the various sensor types described above, we estimate that the different sensors will have different S/N ratios when viewing the same Čerenkov signal under similar background sky conditions as follows:

$$\frac{(S/N)_{PIN}}{(S/N)_{CZ-SI}} = 4$$

and

$$\frac{(S/N)_{PMT}}{(S/N)_{CZ-SI}} = 1300$$

A PIN diode used with a Winston cone to reduce the field of view could have

$$\frac{(S/N)_{PIN}}{(S/N)_{CZ-SI}} = 40$$

Whether to use PIN diodes or solar panels for the detection element depends upon the desired energy threshold; solar panels always give a higher energy threshold in general than PIN diodes, and will require substantially more rigid mechanical attachment to resist strong winds. Solar panels will also receive some signal from through-going ionizing particles from vertical showers, this may complicate the interpretation of the Čerenkov light signal. The solar panel system would also cost more to construct due to the more demanding impedance matching requirements of the front end preamplifier and the higher cost of the panels ($400 per solar panel for 0.4 m^2 effective area vs. $70 each for PIN diodes with 1 cm^2 area). Solar panels, however, can be used for power generation , which PIN diodes cannot accomplish. PIN diodes further will require a small bias voltage, typically 50V. Additional money would need to be invested to construct this power supply.

PMTs would provide the lowest energy threshold of all of the sensors, but the design is complicated by the need for a high voltage (several hundred volts) supply to operate the device. PMTs in general are more fragile and more expensive than PIN diodes (by about a factor of 2). Furthermore, the finite resistivity of the photocathode may cause the response to saturate at moderate light levels. Questions concerning linearity and long term stability need to be addressed. If these difficulties can be addressed, a PMT-based Čerenkov detector would be a viable solution, and would likely meet or exceed the silicon detector performance, except at steep zenith angles.

Rejection of Airplane/Lightning Backgrounds An additional design constraint for optical cosmic ray detectors is the the necessity for eliminating false triggers due to airplanes, lightning and other artificial sources of light pulses. These backgrounds have several features which distinguish themselves from cosmic ray generated Čerenkov light. Some of the characteristics which can be used to reject these background events include periodicity, pulse width, lateral distribution, and wavefront timing. These constraints provide sufficient redundant measurements to unambiguously reject these background events[154]. In order to use these constraints, the electronics data acquisition system would need to provide a waveform digitization of each pulse, with approximately 100 nsec time slice, and about 5 milliseconds long.

A.3 Air Čerenkov Detector Design and Performance

Based upon the considerations of the previous section, we have designed and simulated a strawman air Čerenkov detector. We have chosen a silicon detectors for the baseline design due to their ability to record Čerenkov light from steep zenith angle showers.

A.3.1 Detector Station Description

Optimization of Silicon Sensor Quantity and Orientations In order to keep the air Čerenkov detector costs to a minimum, we optimize the number of sensors and their orientations to yield the best reconstruction of the Čerenkov light direction and amplitude at a given station.

Stations with 4, 5, 6, 7, and 8 sensors were investigated with various sensor orientations. The optimum minimal sensor configuration consisted of 6 sensors, with one sensor oriented vertically, and 5 detectors oriented at a 60 degree tilt to the vertical, and spaced evenly in 72° increments. This is referred to as a (1+5) sensor design with (0°,60°) sensor orientation.

Mechanical Attachment The heavy mass of the water Čerenkov particle detector makes an ideal anchor for a solar panel detector. The panels can be attached to the outside of the water Čerenkov tanks using lightweight steel supports. For PIN diode and PMT sensors, mechanical support considerations will will be substantially easier due to their smaller profiles. In any event, we anticipate that five sensors will be held at 60° tilts with respect to the vertical, with one sensor resting on the top of the tank, pointed vertically.

Data Acquisition System Design Figure A.3 illustrates the general strawman design of the air Čerenkov data acquisition system. The system consist of six sensors, each of which feeds into its own high gain charge-sensitive preamplifier. The output of each preamp feeds into a FADC data recording system. The FADC system record the AC pulse amplitude in 100 nsec bins. The FADC output feeds into a deep buffer ($> 64k$ deep) which allows the pulse shape to be recorded, up to 6 milliseconds long.

A central processor continually reads the aligned buffer memory from each sensor and forms a coincident sum. This summed waveform is then examined using a moving boxcar averager. If the integrated area under the boxcar exceeds a dynamic threshold, the event forms a trigger and the data from each of the 6 sensors is read into a secondary buffer. The time of the crossing over threshold is recorded for the summed data stream.

The trigger bit is sent to the water Čerenkov triggering system and is communicated to the adjacent detectors to see if they have also been triggered by a light pulse. If a several stations have triggered within a predefined time window, all triggering events are instructed to forward the data for the event back to the central station. We anticipate that the air Čerenkov system will trigger itself, or that it will be triggered by a trigger of the water Čerenkov detector. In this manner, we expect that the air Čerenkov system will impose minimal burden of the water Čerenkov system.

Typical data sizes per event are expected to be about 100 Bytes, and individual station alert rates should be on the order of 0.5 Hz (based upon lab studies of sensor noise level in a dark box). A trigger requiring 3 nearest neighbors in a 6 nearest neighbor system to trigger within 100 μ seconds would give a station triggering rate of 0.0014 Hz, and an average data rate of 500 bytes per hour. This data rate is very small compared to the expected data rate for the water Čerenkov detector, and should easily be accommodated by the envisioned communications and triggering system for the water Čerenkov detector.

A.3.2 Expected Performance

We have simulated the performance of a large array of air Čerenkov detectors to examine the angular, energy, and X_{max} resolution as a function of primary energy and S/N ratio using the above system design.

The full simulated detector consist of 1089 stations arranged in a hexagonal close-packed array on a flat plane. The detector is assumed to be located at an altitude of 50 meter above sea level (1030 g cm^{-2}, similar to Woomera, Australia). The spacing between nearest neighbor detectors is 1.5 km. The full detector array is approximately 48 km in the east-west direction, and 42 km in the north-south direction (Figure A.4). Each detector contains the sensors orientation and electronics systems described above.

Events are generated by seeding MOCCA-simulated showers onto the simulated array. Events are analyzed by reconstructing the local Čerenkov light direction at each station using a 'shadow fitting' algorithm. The impact location for the core of the shower is calculated from the mean station position , weighted by the fitted station amplitudes derived in the first stage of reconstruction. A second reconstruction is performed to determine the direction of the original cosmic ray from the individual station directions[155]. The lateral distribution of the Čerenkov photons is reconstructed using the fitted amplitudes, core position, and primary direction. The fitted lateral distribution function is used to calculate $\rho(1200)$ the Čerenkov photon density at a perpendicular distance of 1.2 km from the shower axis, and $\rho(500)/\rho(3000)$. $\rho(500)/\rho(3000)$ is a useful quantity because it is directly correlated with the shower X_{max}.

We present only results for S/N ration of 100 due to space considerations.

Angular Resolution Figure A.5 illustrates the expected angular resolution for the primary cosmic ray direction for a S/N ratio of 100. In general, one has angular resolution of 1-2° for near vertical showers, and 0.3-0.5° for steep zenith angle shower.

The angular resolution expected is similar to or exceeds the resolution expected for the water Čerenkov particle detector array. Even so, it may be possible to use the core from the water Čerenkov particle array detector to substantially improve the angular resolution of the Air Čerenkov detector. Alternatively, the air Čerenkov system can be used to provide geometric information to the nitrogen fluorescence detectors for steeply inclined showers which do not trigger the particle detector array. This information will be crucial for reconstruction of events viewed by only a single nitrogen fluorescence detector, and will therefore provide a different type of 'hybrid reconstruction' capability for these detectors.

Energy Resolution Figure A.6 illustrates the expected energy resolution of the air Čerenkov detector as a function of zenith angle for a S/N ratio of 100. For vertical showers, the energy resolution is about 30-40%, and for steep zenith angles the resolution can be better than 10%. This is because $\rho(1200)$ is optimized for energy resolution at steep zenith angles, at near vertical shower trajectories, the optimal energy measurement distance is close to 100 m from the core. Since the array has 1.5 km spacing between detectors, it is unlikely that a station will be hit within 100 m from the core for a vertical shower. However, one may choose to fit the small *subset* of showers which do have density measurements at this distance, and improve the energy measurement for these events. We have not done this in this analysis. It is unlikely the vertical energy resolution will ever get much better than 40% at 1 ZeV, due to the fact that vertical EAS at these energies can have X_{max} which approach the ground level!

Xmax Resolution In Figure A.7 we show the X_{max} resolution of the simulated array as a function of S/N ratio. The best resolution occurs for zenith angles of 60°, and for S/N ratio > 10.

Detector Angular Acceptance The detector angular acceptance for the simulated detector is summarized in Table A.1. The results are presented in terms of acceptance ($km^2 sr$ of detection aperture per km^2 of ground area of the detector) so that the full aperture is easily calculated by multiplying the the physical ground area of the detector by the angular acceptance. Note that the aperture at 10^{20} eV is approximately π steradians. This is similar to the angular acceptance of the surface array. The difference is that the air Čerenkov aperture is more heavily weighted toward large zenith angles than the water Čerenkov detector. The detection aperture can exceed π steradians because showers hitting outside of the physical detector dimensions can also trigger the array, especially at large zenith angle trajectories.

Expected Cost A preliminary cost estimate, based upon using numbers derived for the particle array triggering and communications scheme, has been performed. CZ-SI or PMT sensor systems can be expected to cost about \$6k/station (standalone system with no Auger array), or about \$3.5k/station (add-on to Auger particle detector array). A PIN diode sensor system would cost about \$3.5k/station (standalone system with no Auger array) or about \$1.0k/station (add-on to Auger particle detector array). In either case, the air Čerenkov system can provide enhanced measurement capabilities at an inexpensive cost.

Summary The resolution of an Air Čerenkov detector array over most of the zenith angle ranges is similar to or better than that which is expected for a 1.5 km spacing array of particle detectors. The energy threshold for a silicon detector PIN diode sensor-based system will be dominated during the moonless nights by electronic noise levels, and during other times by fluctuations in the background light level (full moon, or daytime sky background). We estimate that a 1.5 km spacing air Čerenkov array with Cz-Si panel light detectors will have a night operation threshold of 30 EeV, assuming a minimum S/N level of 10 at 1 km from the core for satisfactory performance. The daytime operation threshold, for indirect sunlight, will be about 50-60 EeV. For PIN diode sensors, the nighttime threshold will be about 5-8 EeV, and with PMT sensors the threshold could be below 1 EeV. Other detectors using Winston Cones with more sensors could show lower energy thresholds, and correspondingly better performance (better S/N ratio for the same energy cosmic ray). The PIN diode sensor detector should be able to provide a 40% duty cycle for 10^{20} eV cosmic rays, and 80% for 10^{21} eV particles.

The main obstacle to development of this system is the newness of the technique. Barring unforseen obstacles, the realization of an air Čerenkov array with substantially increased duty cycle should be possible in the near future. The construction and successful operation of a prototype system in the near future, especially in coincidence with either the AGASA or HiRes detectors, would help to confirm the expected sensitivities expected from the design study.

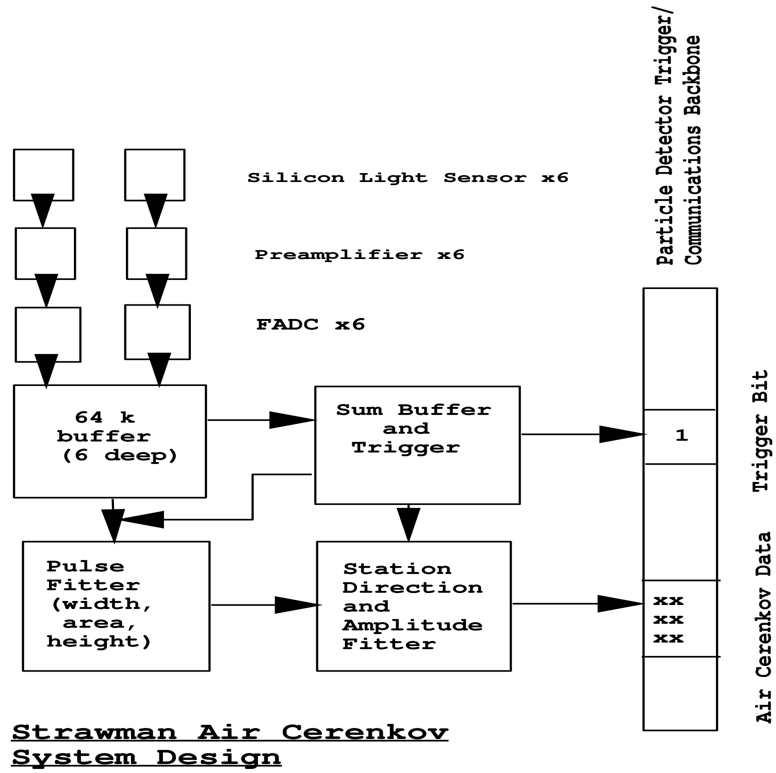

Figure A.3: Strawman Data Acquisition System

Energy (EeV)	S/N ratio	Acceptance (sr)
10	10	1.36
10	100	1.36
100	10	3.13
100	100	3.23
100	1000	3.32
1000	10	1.72
1000	100	3.75
1000	1000	3.74

Table A.1: Detector Angular Acceptance as a function of primary energy and S/N ratio.

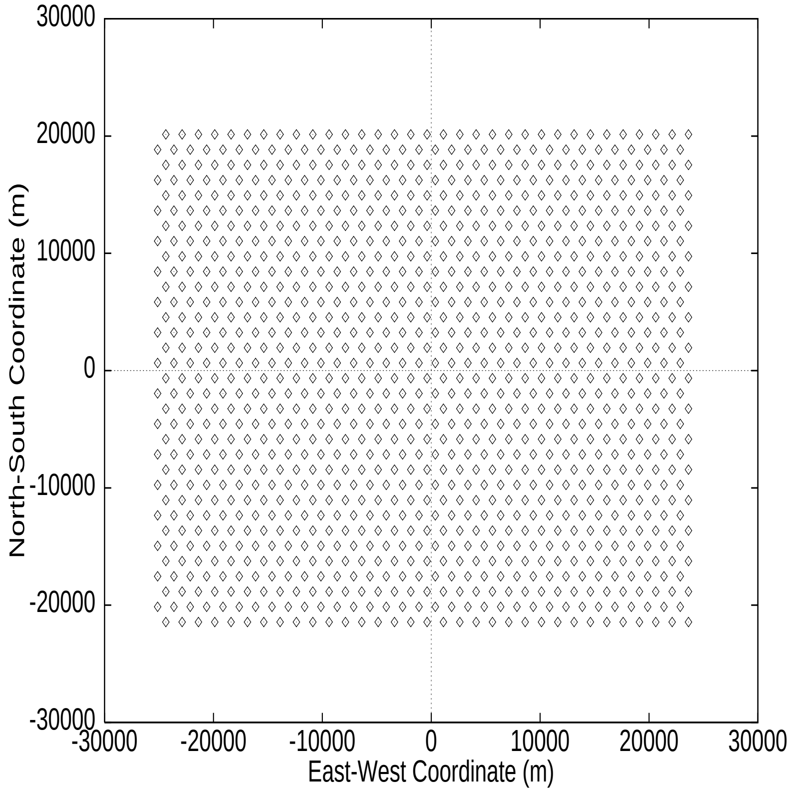

Figure A.4: Air Čerenkov station layout for performance simulation. Each diamond represents a single 6-sensor detection station. Horizontal Axis: distance (m); Vertical Axis: Distance(m).

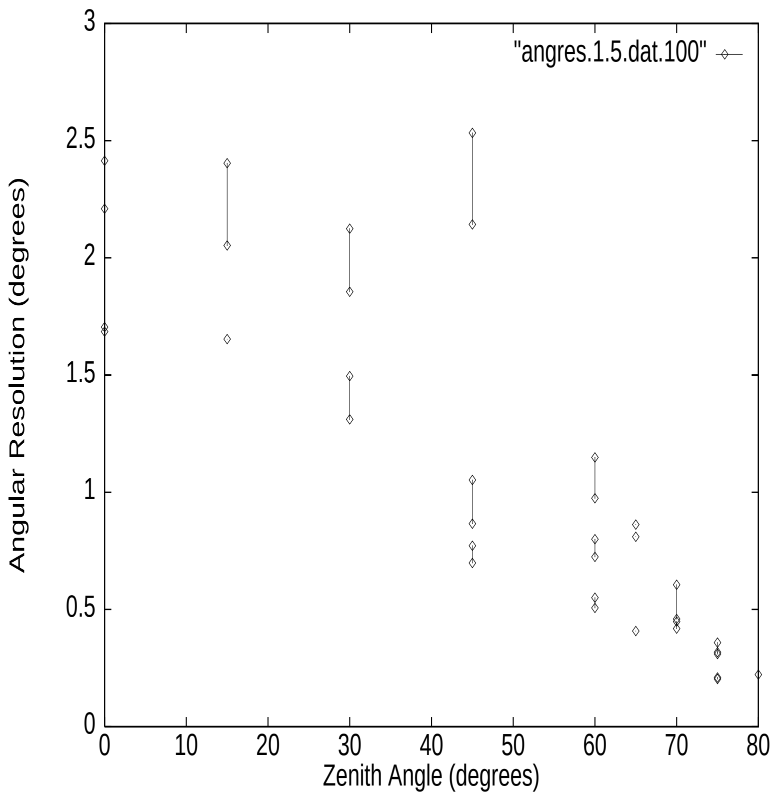

Figure A.5: Expected Angular Resolution of Original Primary direction as a function of Zenith angle for various cosmic ray energies for fixed S/N ratio of 100. For each zenith angle, several points/bars are plotted. For angles with 3 distinct points/bars, the smallest error point is for 1 ZeV, next smallest error is for 100 EeV, largest error is for 10 EeV. For Two points/bars plotted, smallest error is for 1 ZeV, and the second point is for 100 EeV. Horizontal Axis: Zenith Angle (degrees); Vertical Axis: 1 σ angular Resolution (degrees).

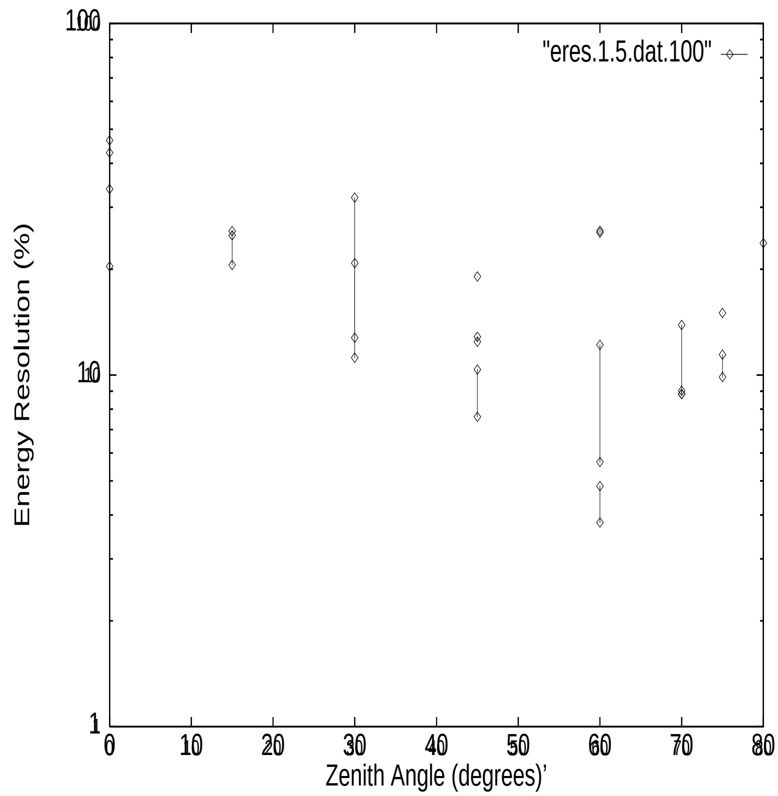

Figure A.6: Expected Energy Resolution as a function of Zenith angle for various cosmic ray energies for fixed S/N ratio of 100. For each zenith angle, several points/bars are plotted. For angles with 3 distinct points/bars, the smallest error point is for 1 ZeV, next smallest error is for 100 EeV, largest error is for 10 EeV. For Two points/bars plotted, smallest error is for 1 ZeV, and the second point is for 100 EeV. Horizontal Axis: Zenith Angle (degrees); Vertical Axis: 1 σ Energy Resolution (%).

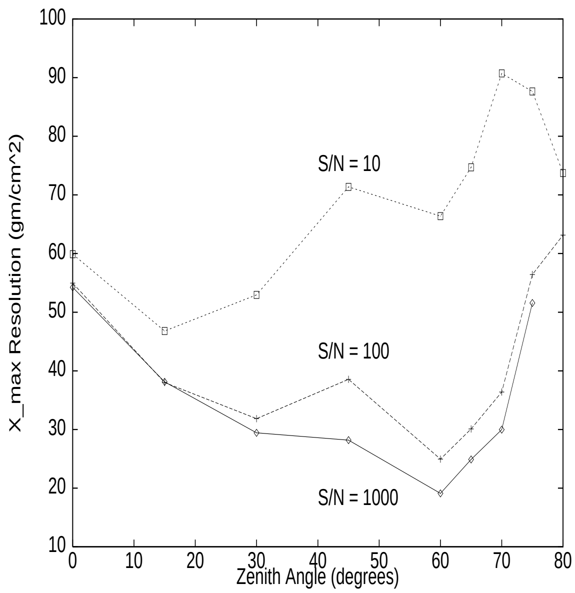

Figure A.7: Expected X_{max}Resolution as a function of Zenith angle for various S/N ratios as a function of Zenith angle. Horizontal Axis: Zenith Angle (degrees); Vertical Axis: X_{max}resolution (g cm^{-2})